International Journal of Biochemistry and Cell Biology 114 (2019) 105554

Contents lists available at ScienceDirect

International Journal of Biochemistry and Cell Biology

journal homepage: www.elsevier.com/locate/biocel

Targeted gold nanoparticles enable molecular CT imaging of head and neck cancer: An *in vivo* study

Sara Khademi[a], Saeed Sarkar[b], Ali Shakeri-Zadeh[c], Neda Attaran[d], Sharmin Kharrazi[e], Mohammad Reza Ay[b], Hosein Azimian[f], Hossein Ghadiri[b,*]

[a] Department of Radiology Technology, School of Paramedical Sciences, Mashhad University of Medical Sciences, Mashhad, Iran
[b] Department of Medical Physics and Biomedical Engineering, Tehran University of Medical Sciences, Tehran, Iran
[c] Medical Physics Department, School of Medicine, Iran University of Medical Sciences (IUMS), Tehran, Iran
[d] Department of Medical Nanotechnology, Applied Biophotonics Research Center, Science and Research Branch, Islamic Azad University, Tehran, Iran
[e] Department of Medical Nanotechnology, School of Advanced Technologies in Medicine, Tehran University of Medical Sciences, Tehran, Iran
[f] Medical Physics Research Center, Mashhad University of Medical Sciences, Mashhad, Iran

ARTICLE INFO

Keywords:
Molecular CT imaging
Folic acid
Gold nanoparticles
Cancer

ABSTRACT

The development of various cost-effective multifunctional contrast agent for specific targeting molecular imaging of tumors presents a great challenge. We report here the *in vivo* targeting imaging of folic acid (FA) gold nanoparticles (AuNPs) through cysteamine (Cys) linking for targeted of human nasopharyngeal head and neck cancer by computed tomography (CT). The toxicity of nanoparticles in kidney, heart, spleen, brain and liver was evaluated by H&E (hematoxylin and eosin) assay. We showed that the formed FA-Cys-AuNPs with an Au core size of ~13 nm are non-cytotoxic in the particle concentration of 3×10^3 μg/ ml. The nude mice were scanned using a 64-slice CT scan with parameters (80 kVp, slice thickness: 0.625 mm, mAs: 200, pitch: 1). CT scan was performed before and after (Three and six hours) I.V (Intra Venous) injection of AuNPs and FA-Cys-AuNPs. The distribution of nanoparticles in the nude mice was evaluated by imaging and coupled plasma optical emission spectrometry (ICP-OES) analysis. The findings clearly illustrated that a small tumor, which is undetectable via computed tomography, is enhanced by X-ray attenuation and becomes visible (4.30-times) by the molecularly targeted AuNPs. It was further demonstrated that active tumor cells targeting (FA-Cys-AuNPs) is more specific and efficient (2.03-times) than passive targeting AuNPs. According to the results, FA-Cys-AuNPs can be employed as a promising contrast agent in CT scan imaging and maybe in radiotherapy that require enhanced radiation dose.

1. Introduction

In 2005, molecular imaging techniques were defined as the techniques that enable us to directly or indirectly monitor and record the temporal-spatial molecular distribution or cellular processes for biochemical, biological, diagnostic and therapeutic applications(Mao et al., 2018; Thakur and Lentle, 2005). In 2007, molecular imaging was recommended to the Nuclear Medicine Society (NMS) where molecular imaging could measure and monitor biological processes and display biological features at the cellular and molecular levels in humans and other living organisms (Mankoff, 2007). Presently, the molecular imaging methods that are used include: nuclear medicine, magnetic resonance imaging (MRI), fluorescence imaging, and computed tomography (CT). The major concern associated with fluorescence imaging the lower spatial resolution of fluorescence, the limited tissue penetration depth, which limited their further applications in vivo study and cannot provide 3D tissue detail. MR imaging is a noninvasive and powerful imaging technology able to realize multi-parameter imaging. It is free from ionizing radiation and good for soft tissue imaging, but disadvantages include the expense and long scan time. CT scan has a better spatial and density resolution, lower cost and higher accessibility, allows three-dimensional visual reconstructions of tissue, requires less time for imaging and the most commonly utilized diagnostic tool in clinic (Abed et al., 2019; Huang et al., 2019; Jiang et al., 2017; Keshavarz et al., 2018; Lee et al., 2013; Long et al., 2016; Xu et al., 2017; Zhang et al., 2015). A better resolution, especially when imaging the head and neck, is much more revealing. Head and neck tumor, especially nasopharyngeal (KB cells), is one of the most undetectable tumors in the head and neck region, which is often confused with many illnesses. So, there is need for a diagnostic method that

* Corresponding author.
E-mail address: h-ghadiri@sina.tums.ac.ir (H. Ghadiri).

https://doi.org/10.1016/j.biocel.2019.06.002
Received 29 January 2019; Received in revised form 7 June 2019; Accepted 10 June 2019
Available online 02 July 2019

recognizes the tumor at an early stage. Contrast agents are often required for effective CT scan imaging. Today, iodine contrasts are used for CT scan imaging, which are eliminated from the bloodstream in a short period of time, so the physician has little time for imaging and may need to use further contrast. The iodine contrasts are distributed throughout the body evenly and do not specifically target the tumor (Hainfeld et al., 2006). Among all metals with high atomic number, we have chosen the gold nanoparticles (AuNPs) as they have a better biocompatibility and high circulation time as a result of more molecular weight than iodine. They also have a higher atomic number than iodine due to weakening of X-ray intensity, and simpler surface chemistry due to their attachment to other ligands (Beik et al., 2017). Due to the targeting of AuNPs by other ligands, vitamins or genes etc., we have shifted our focus toward molecular imaging. In this study, folic acid (FA) was used to confer targeting ability to AuNPs. FA is a type of vitamin with a molecular weight of 480 Daltons. Cancer cells require more FA vitamin due to their higher metabolism, and there is more FA receptor on the surface of tumor cells than normal cells (Beik et al., 2017; Missbach-Guentner et al., 2011; Samadian et al., 2016). For this reason, FA as a targeting factor has been attached to AuNPs by cysteamine (Cys) linker. Cys is a type of non-toxic linker, which easily attaches itself to AuNPs due to its SH group and does not require prethiolation. On the other hand, the other end of Cys is amino group, which is easily attached to the carboxylic group of FA. Therefore, FA makes targeted imaging possible. In the previous study (Khademi et al., 2018a), AuNPs attached to folic acid via cysteamine (FA-Cys-AuNPs) were well synthesized, and characterization tests, including UV–vis, Transmission electron microscopy (TEM), FTIR, and ICP-OES were carried out. In addition, the AuNPs and FA-Cys-AuNPs with the size of 13 and 15 nm were synthesized. Then, the toxicity of the nanoparticles was measured at the concentrations of 0–500 μM by flow cytometry, colony, MTT, and H&E assays, which indicated no toxicity. Weakening X-radiation tests were performed in the *in vitro* model. The development of various easy approaches to produce targeted gold NPs with improved cytocompatibility remains a great challenge. Literature reports have shown that by conjugating onto the surface of the gold NPs, targeted CT imaging of tumor in vivo can be achieved. In this study, we tried to show the presence of AuNPs and FA-Cys-AuNPs in the *in vivo* model by using molecular CT imaging. Before imaging, folic acid-bound nanoparticles were injected into a mice and its toxicity in the brain, heart, kidney, liver and spleen was assessed by histopathology assay, which showed no toxicity at all. Imaging of the animal was performed before the injection, and 3 and 6 h after the injection of AuNPs and FA-Cys-AuNPs, which showed a greater amount of AuNPs in the tumor at 3 h after the injection than 6 h. On the other hand, the presence of FA-Cys-AuNPs resulted in a 2.03-fold increase in the attenuation of X-rays compared to AuNPs in the tumor. Six hours after the injection, the nanoparticles were separated from the organ and the ICP-OES test was performed to evaluate the distribution of nanoparticles in different organs. The results showed that, most of FA-Cys-AuNPs were present in the tumor, and the rest were present in the liver, lungs, spleen and kidney of the animal.

2. Materials and methods

2.1. Materials

Water used in all the experiments was purified using a Milli-Q Plus 185 water purification system (Millipore, Bedford, MA) with a resistivity of 18.2 MΩ cm. Cell culture was done according to the previous study (Khademi et al., 2018a). In brief, KB cells and human dermal fibroblasts (HDFs) were acquired from Pasteur Institute in Tehran, Iran and cultured in DMEM medium with 10% FBS, incubator temperature of 37 °C and 5% CO_2. MTT, folic acid (FA), gold salt ($HAuCl_4$), dimethyl sulfoxide (DMSO) were obtained from Sigma Aldrich, USA.

2.2. Synthesis of gold nanoparticles attached to folic acid

2.2.1. Preparation of folic acid-bound cysteamine

Synthesis of gold nanoparticles attached to folic acid was performed according to the previous study (Khademi et al., 2018a). In brief, the activated folic acid N-hydroxysuccinimide (FA-NHS) was synthesized using the Van Steenis and Peggy Chan method with a little modification (Chan et al., 2007). Initially, the dimethyl sulfoxide (DMSO) and triethylamine solution underwent heater stirrer at 100 to 1 ratio for 10 min. Then, 0.25 g of FA was added to the mixture in a very gradual process and underwent heater stirrer in a dark condition for one night. FA was then subjected to heater stirrer with 0.1 g of dicyclohexylcarbodiimide and 0.1 g of N-hydroxysuccinimide for 24 h. Then, the dicyclohexylurea (DCU) was filtered off and DMSO and triethylamine were also removed due to vacuum toxicity. In the second step, to prepare the FA attached to the cysteamine (Cys), the FA attached to the NHS was dissolved in a mixture of 2 to 1 DMSO and triethylamine, and 0.1 g of Cys was added to the mixture under stirrer and was subjected to heater stirrer for 24 h. The resulting yellow solution was filtered and washed twice with ethylether. Cys is an ideal non-toxic linker and an effective material in the treatment of neurological disorders. Cys also acts as one of the important factors in the metabolism of the body. Considering the presence of amine group at the Cys level, it has the possibility to attach to the carboxylic group of FA. On the other hand, it facilitates the attachment of SH (thiol) Cys to gold group, so it does not require etiolation. The thiol group produces sulfhydryl bond with gold.

2.2.2. Attaching the gold nanoparticles to folic acid bound cysteamine (FA-Cys-AuNPs)

Attaching the gold nanoparticles to the folic acid bound cysteamine (FA-Cys-AuNPs) was accomplished in two steps (Gao et al., 2012):

First step: The AuNPs were synthesized: First, all containers were washed with solution (3 to 1 solution of chloride acid to nitric acid) and washed by distilled water and dried in an oven. Then, the mixture containing 5 ml of gold salt ($HAuCl_4$) and 90 ml of deionized water was placed in a 3 valve balloon and underwent heater stirrer. When the solution reached boiling temperature, 5 ml of sodium citrate trihydrate was added quickly. The color of the solution turned from pale yellow to red. After observing the change in color, the solution remained under steady temperature for another 15 min.

The second stage, after cooling of the produced spherical nanoparticles, the FA attached to Cys, which was dried, was added to the solution gradually and was kept under heater stirrer for another 4 h. Then, to remove excess toxic substances, the produced solution was purified by centrifugation and washed twice with deionized water.

2.3. Characterization techniques

TEM was performed using a Zeiss EM 900 and used to investigate morphology and size of AuNPs. UV–vis spectra were recorded using a SPEKOL 2000 (Analytik Jena, UK) spectrophotometer. The concentrations of AuNPs in μg/ml were measured by the ICP-OES.

2.4. In vivo CT imaging of a KB tumor model

Animal experiments and animal care were done according to protocols approved by the Ethics Committee for Animals, in accordance with the laws of National Ministry of Health. Four to six weeks nude male mice were subcutaneously injected with 10×10^6 cells per mice in the back of the right leg. When tumor size reached 0.1 cm^3 after 3 weeks, the mice were scanned using a 64-slice CT scan (GE, imam Khomeini hospital) with parameters (80 kVp, slice thickness: 0.625 mm, mAs: 200, pitch: 1). CT scan was performed before and after IV (intra venous) injection with a concentration of 3×10^3 μg/ ml AuNPs and FA-Cys-AuNPs. Three and six hours after the injection, imaging was performed and the distribution of nanoparticles in the

mice was evaluated.

2.5. In vivo bio-distribution of AuNPs and FA-Cys-AuNPs after intravenous injection

Six hours after the injection of AuNPs and FA-Cys-AuNPs in the animals and CT scan imaging, the mice were killed. Then their tumor, liver, lungs, heart, left and right kidneys and spleen were removed and weighed. The organs were cut into 1–2 mm slices and were incubated in aquilegia solution for 4 h. The amount of gold in different organs was measured by ICP-OES.

2.6. Histological studies

To investigate the toxicity of FA-Cys-AuNPs in different organs of the mice, the mice were killed 2 weeks after the injection of AuNPs and their liver, brain, spleen, and kidney were quickly separated and placed in 10% formalin buffer solution. The organs were hydrated and embedded with paraffin. Paraffin-embedded specimens were cut into 3 mm slices by microtome. Sections were then washed with PBS. For H& E (hematoxylin and eosin assay), the organs were placed in a Coplin jar containing hematoxylin for 2–3 min. Then, the specimens were washed with water and placed in 1% eosin Y solution for one minute. Finally, the cover slips were hydrated and placed on the slides before being observed with an optical microscope.

2.7. Statistical analysis

One-way analysis of variance (ANOVA) was used to determine the significance level of the obtained data. P-value of less than 0.05 was considered as the level of statistical significance.

3. Results and discussion

3.1. Synthesis and characterization FA-Cys-AuNPs and AuNPs

In the previous study, the AuNPs and FA-Cys-AuNPs were synthesized and reported (Khademi et al., 2018b). In this section, the results of injection of AuNPs and FA-Cys-AuNPs in the nude mice model are investigated. AuNPs suspensions were synthesized by the protocols described before. UV–vis spectroscopy and TEM images are presented in Fig. 1. UV–vis spectrometry was utilized to characterize the synthesized FA-Cys-AuNPs. It is clear that the FA-Cys-AuNPs displays a typical surface plasmon broadened band at 705 nm, indicative of the formation of AuNPs (the unmodified AuNPs display a characteristic surface plasmon absorption at 520 nm). The size and morphology of the formed nanoprobe were characterized using TEM (Mohandes and Salavati-Niasari, 2014a, 2014b) (Fig. 1). It can be noted that the formed FA-Cys-AuNPs has a spherical shape with mean diameter of ˜15 nm.

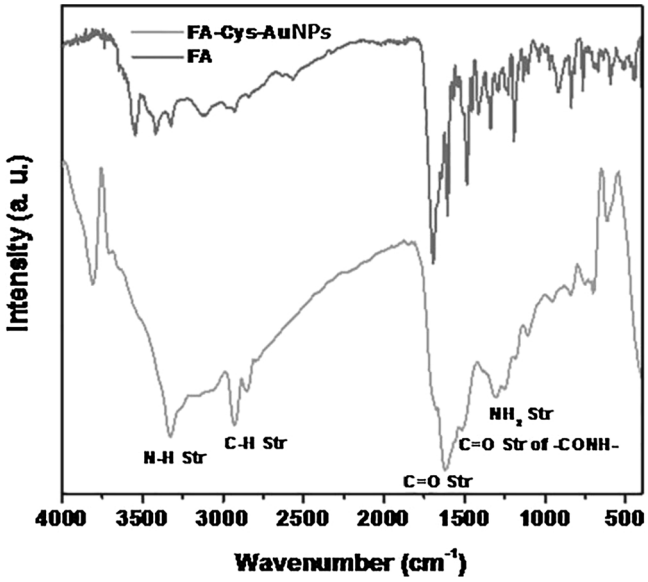

Fig. 2. Fourier transform infrared (FTIR) spectra of FA-Cys-AuNPs and FA.

Conjugation of folic acid to AuNPs was verified by comparing the FTIR spectra of FA-Cys-AuNPs and FA (Fig. 2); the band at 1315 cm^{-1} corresponds to asymmetric stretching vibration of -NH2 in folic acid and at 1627 cm^{-1} and 1677 cm^{-1} relate to C—O stretching in carboxyl acids. While the band at 1516 cm^{-1} belongs to the C—O bond stretching vibration of —CONH-group. The bands between 3000 and 3500 cm^{-1} are due to the O—H stretching and NH-stretching vibration bands of FA and Cys, respectively (Khademi et al., 2018a). In addition, the absence of absorption band at 2100–2300 cm^{-1} is attributed to characteristic absorption of —SH of cysteamine to the surface of AuNPs, suggesting that -SH coordinates with Au on the surface of the particles. The band at 2850–2927 cm^{-1} relates to asymmetric and symmetric C—H stretching vibrations of —CH2.

3.2. Cytocompatibility assays

We evaluated the effects of incubation time on toxicity of KB and HDF cells at different time point (6, 12, and 24 h; Fig. 3) and found that cell viability by MTT assay (Amiri et al., 2018) of KB and HDF cells decreased with increasing time point, but it was not significant. These results propose good cytocompatibility of the FA-Cys-AuNPs.

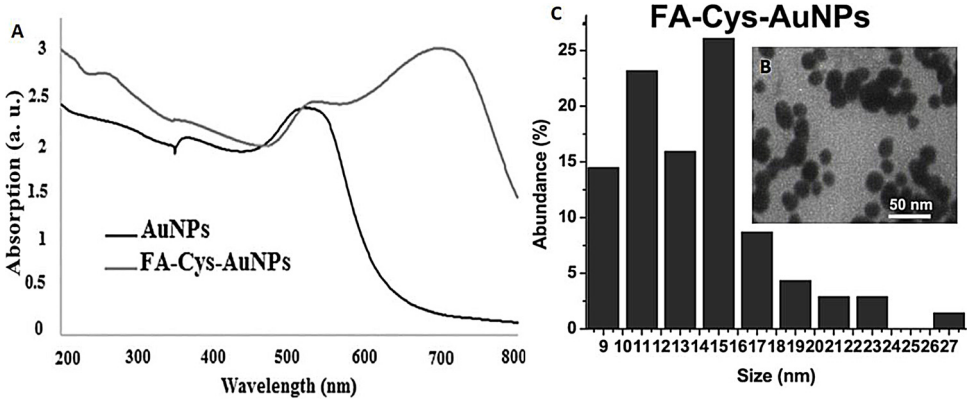

Fig. 1. UV–vis spectra showing a shift in the surface plasmon resonance of AuNPs due to adsorption of FA-Cys (A). TEM images (B) and size distributions of Cys-AuNPs (C).

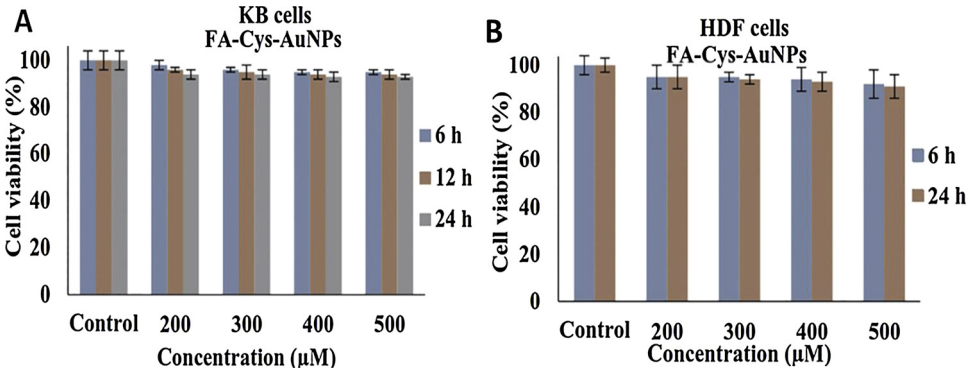

Fig. 3. (A) MTT viability of KB cells (a) and HDF cells after treatment with FA-Cys-AuNPs at different concentrations (0–500 μM) (n = 3).

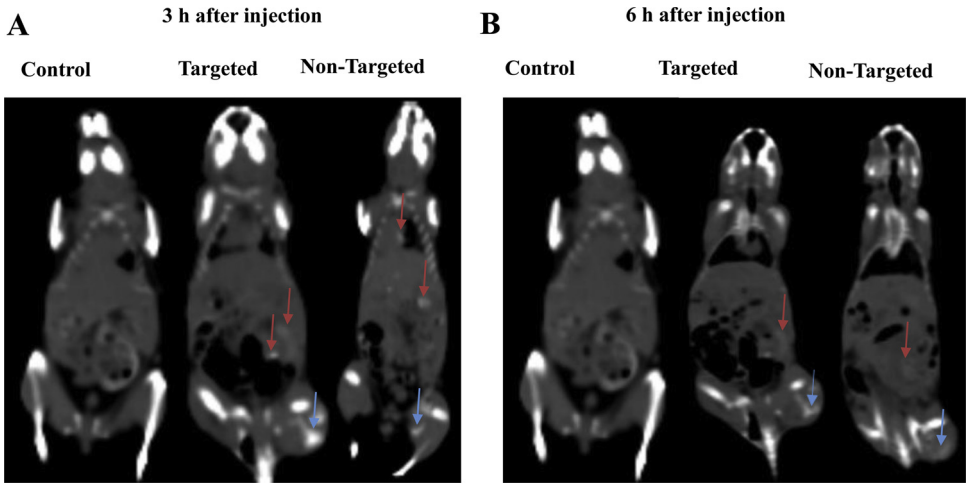

Fig. 4. Coronal CT images of nude mice after IV injection of AuNPs and FA-Cys-AuNPs at 3 h (A) and 6 h (B) after injection (blue arrows).

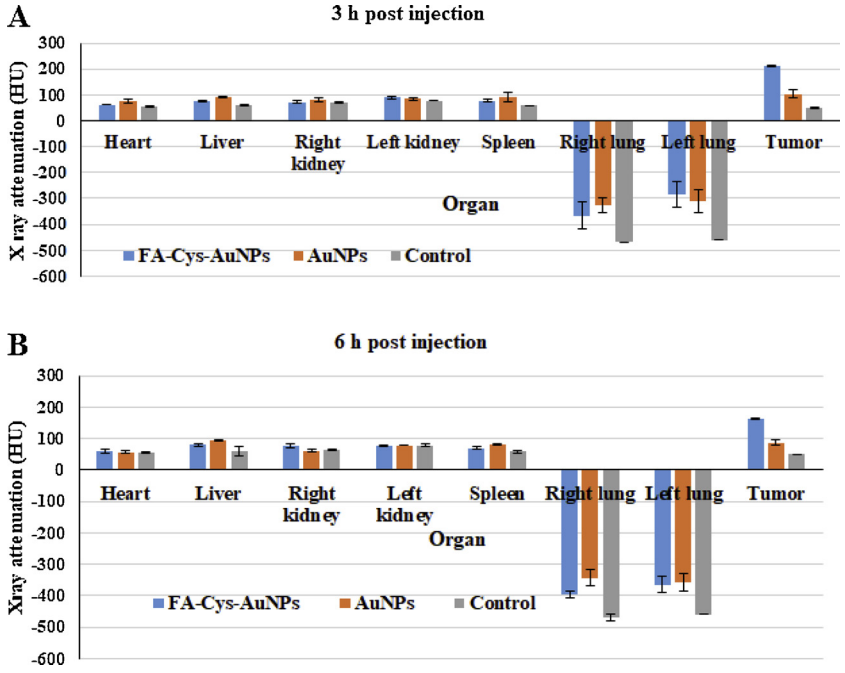

Fig. 5. X ray attenuation of AuNPs and FA-CysAuNPs in various organs after 3 h (A) and 6 h (B) after IV injection.

Table 1
Summary of *in vivo* studies in which FA-AuNPs have been used as a CT contrast agent.

Reference	Size (nm)	Time point (h)	Tumor model	X-ray Energy (kVp)	Delivery method	CT number enhancement		
						(Au v.s. control)	(F-Au v.s. control)	(F-Au v.s. Au)
Wang et al. (2013)	3	6	Lung adenocarcinoma	80	I.V	NI	2	NI
					I.P	NI	1.50	NI
Liu et al. (2013)	5	1	Nasopharyngeal adenocarcinoma	120	I.V	1.30	1.45	1.15
Chen et al. (2013)	4	24	Nasopharyngeal adenocarcinoma	80	I.V	1.07	2.50	2.06
Peng et al. (2013)	3	6	Nasopharyngeal adenocarcinoma	100	I.V	1.28	2	1.16
					I.P	1.24	2	1.14
Zhou et al. (2016)	2	2.5	Nasopharyngeal adenocarcinoma	80	I.T	6.05	6.90	1.20
Lu et al. (2016)	6	6	Human Cervical Cancer (Hela cells)	100	I.V	1.30	1.50	1.15
This study	13	3	Nasopharyngeal adenocarcinoma	80	I.V	2.11	4.30	2.03
This study	13	6	Nasopharyngeal adenocarcinoma	80	I.V	1.77	3.30	1.85

I.P: Intraperitoneal; I.V: Intravenous; I.T: Intratumoral; Time point stands for the time interval between nanoparticles injection and CT imaging. *"NI" indicates Not Informed.*

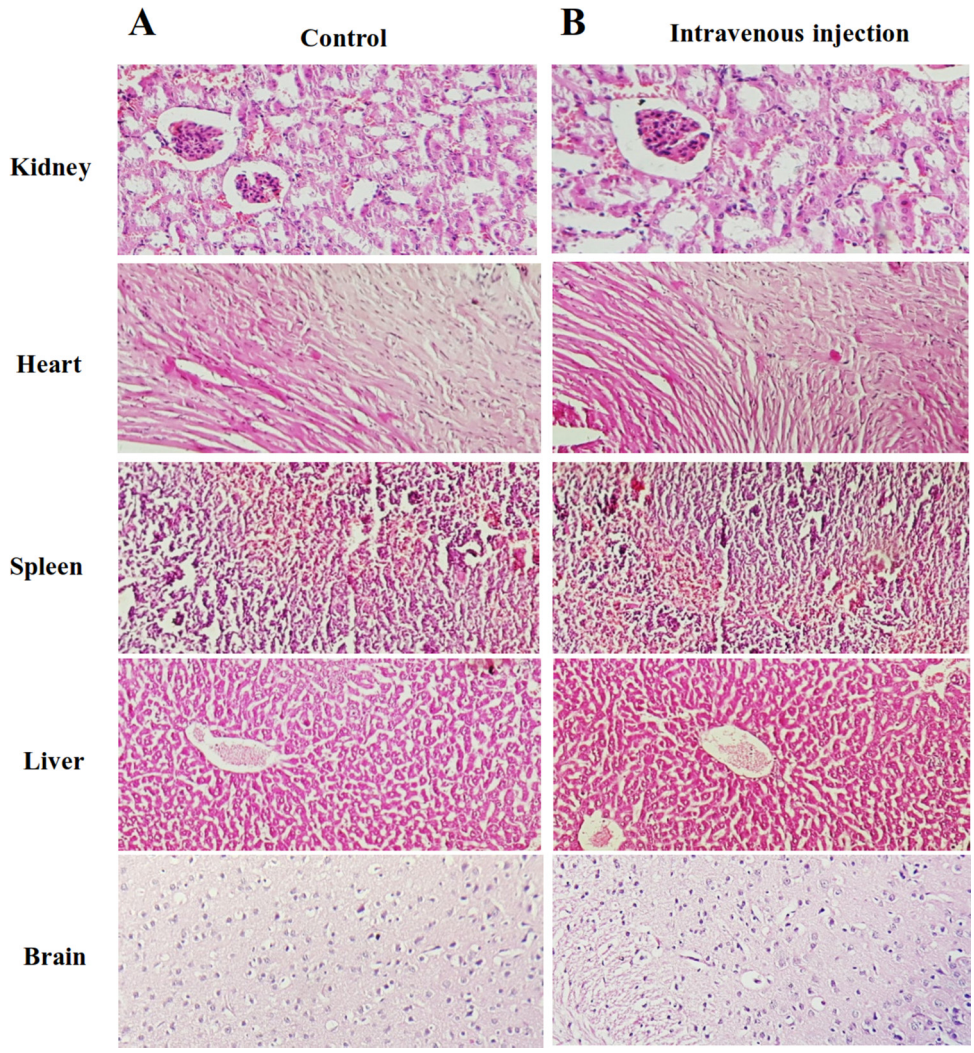

Fig. 6. H&E staining of the various organs in nude mice before (A) and after (B) injection of FA-Cys-AuNPs after 2 weeks.

3.3. Targeted CT imaging of a KB xenografted tumor model in vivo

We next explored the possibility to use the formed FA-Cys-AuNPs for targeted and non-targeted AuNPs CT imaging of tumor cells in vivo. After intravenous injection of the targeted FA-Cys-AuNPs and non-targeted AuNPs, the mice were scanned using a CT system at different time points. Fig. 3 shows the representative coronal sectional CT images and CT values of the KB tumor in nude mice before and after injection with FA-Cys-AuNPs and AuNPs (3×10^3 μg/ ml, 200 μL) via intravenous administration at 3, and 6 h post injection. It can be seen in Fig. 4(A, B) that in all cases, the injection of the AuNPs (either non-targeted or targeted) leads to enhanced CT contrast of the tumor area,

Table 2
In vivo biodistribution of AuNPs and FA-Cys-AuNPs after intravenous injection at 3×10^3 μg/ml concentration.

Tissue	Au Mass per gram of tissue (ppm)	
	Non-Targeted	Targeted
Heart	41.50±3.50	28.58±18.28
Spleen	88.50±4.50	73.47±5.47
Liver	116.80±3.19	90.00±10.00
Lung	171.50±3.50	142.50±10.50
Right kidney	47.49±1.69	33.62±5.84
Left kidney	59.77±8.23	28.61±5.09
Tumor	547.65±392.10	848.90±109.13

and 3 h post injection enables the maximum CT enhancement of the tumor area. When the FA-Cys-AuNPs were injected to the mice, the amount of attenuation in X-ray intensity was about 2.03 times more compared to a group of AuNPs alone. Due to the abundance of folic acid receptor on the surface of the tumor cells, AuNPs enter the cell through endocytosis process, resulting in an increase in the attenuation of X-ray intensity. AuNPs that have not been given a targeting ability increased the passive intensity of X-ray through the enhanced permeation and retention (EPR) phenomenon. The results showed that, with increasing time after the injection, the amount of attenuation in X-ray intensity decreased in the tumor.

Fig. 5(A, B) shows the amount of attenuation in X-ray intensity in various organs. In both cases, the AuNPs and the FA-Cys-AuNPs, the highest levels of attenuation in X-ray intensity are seen.

In order to compare this study with other studies, Table 1 is summarized. In this table, size of nanoparticles, time point, delivery method, tumor model, X-ray energy and CT number enhancement of AuNPs with and without FA in different studies are compared (Chen et al., 2013; Liu et al., 2013; Lu et al., 2016; Wang et al., 2013; Zhou et al., 2016). Our results clearly indicate that the developed FA-Cys-AuNPs have great potential to be used as promising contrast agent for targeted CT imaging of cancer cells. It is important to note that these findings were obtained using a clinical CT scan, which has a relativity low resolution (0.625 mm) compared to micro-CT (45 μM) resolution; so, as micro-CT has not been actually used in medicine, these results have a high potential for clinical applications.

3.4. Histological studies

To investigate the influence and metabolism of FA-Cys-AuNPs (3×10^3 μg/ ml, 200 mL) in healthy BALB/C nude mice after intravenous injection for one month, HE staining of tissue section of major organs (kidney, heart, spleen, brain and liver) were performed and observed using an optical microscope (Fig. 6). Compared to the control group without treatment, the morphologies of major organs do not seem to have appreciable changes and had no significant difference with the control group, suggesting that the injected FA-Cys-AuNPs with an Au core size of ˜13 nm via intravenous injection do not display apparent in vivo toxicity to the organs.

3.5. In vivo biodistribution of AuNPs and FA-Cys-AuNPs after intravenous injection

The results indicated the highest tissue intake at 6 h after injection of AuNPs to tumor, lung, liver, spleen, left kidney, right kidney and heart, respectively, and also 6 h after injection of FA-Cys-AuNPs to tumor, lung, liver, right kidney, left kidney, spleen and heart (Table 2). In both of nanoparticles tumor has the highest Au Mass per gram of tissue (ppm) through ICP (Mohandes and Salavati-Niasari, 2014a, 2014b) analysis.

4. Conclusion

In summary, the FA-Cys-AuNPs, with a size of 15 nm, were well synthesized in the previous study. In this study, the toxicity of nanoparticles with a concentration of 3×10^3 μg/ ml in different organs of nude mice was investigated by histopathologic testing. FA-Cys-AuNPs in different organs of the mice were non-toxic and had a good biocompatibility. The amount of attenuation in X-ray intensity in the presence of AuNPs and FA-Cys-AuNPs in an animal's KB tumor showed that, targeted AuNPs were able to attenuate X-ray intensity by about 2.03 times that of AuNPs. On the other hand, with an increase in time after the injection from 3 to 6 h, the intensity of X-radiation decreased in the tumor. Therefore, due to the increase in the amount of attenuation in X-ray intensity in the presence of FA-Cys-AuNPs and their good biocompatibility, these nanoparticles can be used as effective nanoprobes for targeted imaging. On the other hand, this nanoparticle can be used in radiotherapy where it is necessary to increase the intensity of X-rays for treatment.

Compliance with ethical standards

All mice used in this study were maintained under protocols approved by the Iran County Animal Ethics board (approval number IR.TUMS.MEDICINE.REC.1395.228).

Acknowledgments

The authors gratefully acknowledge Research Center for Molecular and Cellular Imaging (RCMCI), Tehran University of Medical Sciences, Tehran, Iran. This research was supported by grant number 30853 from the Tehran University of Medical Sciences. Tehran, Iran.

References

Abed, Z., Beik, J., Laurent, S., Eslahi, N., Khani, T., Davani, E.S., et al., 2019. Iron oxide–gold core–shell nano-theranostic for magnetically targeted photothermal therapy under magnetic resonance imaging guidance. J. Cancer Res. Clin. Oncol. 1–7.
Amiri, M., Pardakhti, A., Ahmadi-Zeidabadi, M., Akbari, A., Salavati-Niasari, M., 2018. Magnetic nickel ferrite nanoparticles: green synthesis by Urtica and therapeutic effect of frequency magnetic field on creating cytotoxic response in neural cell lines. Colloids Surf. B Biointerfaces 172, 244–253.
Beik, J., Khademi, S., Attaran, N., Sarkar, S., Shakeri-Zadeh, A., Ghaznavi, H., Ghadiri, H., 2017. A nanotechnology-based strategy to increase the efficiency of cancer diagnosis and therapy: folate-conjugated gold nanoparticles. Curr. Med. Chem. 24, 4399–4416.
Chan, P., Kurisawa, M., Chung, J.E., Yang, Y.-Y., 2007. Synthesis and characterization of chitosan-g-poly (ethylene glycol)-folate as a non-viral carrier for tumor-targeted gene delivery. Biomaterials 28, 540–549.
Chen, Q., Li, K., Wen, S., Liu, H., Peng, C., Cai, H., et al., 2013. Targeted CT/MR dual mode imaging of tumors using multifunctional dendrimer-entrapped gold nanoparticles. Biomaterials 34, 5200–5209.
Gao, J., Huang, X., Liu, H., Zan, F., Ren, J., 2012. Colloidal stability of gold nanoparticles modified with thiol compounds: bioconjugation and application in cancer cell imaging. Langmuir 28, 4464–4471.
Hainfeld, J., Slatkin, D., Focella, T., Smilowitz, H., 2006. Gold nanoparticles: a new X-ray contrast agent. Br. J. Radiol. 79, 248–253.
Huang, L., Yang, S., Chen, J., Tian, J., Huang, Q., Huang, H., et al., 2019. A facile surface modification strategy for fabrication of fluorescent silica nanoparticles with the aggregation-induced emission dye through surface-initiated cationic ring opening polymerization. Mater. Sci. Eng. C 94, 270–278.
Jiang, R., Liu, H., Liu, M., Tian, J., Huang, Q., Huang, H., et al., 2017. A facile one-pot Mannich reaction for the construction of fluorescent polymeric nanoparticles with aggregation-induced emission feature and their biological imaging. Mater. Sci. Eng. C 81, 416–421.
Keshavarz, M., Moloudi, K., Paydar, R., Abed, Z., Beik, J., Ghaznavi, H., Shakeri-Zadeh, A., 2018. Alginate hydrogel co-loaded with cisplatin and gold nanoparticles for computed tomography image-guided chemotherapy. J. Biomater. Appl. 33, 161–169.
Khademi, S., Sarkar, S., Shakeri-Zadeh, A., Attaran, N., Kharrazi, S., Ay, M.R., Ghadiri, H., 2018a. Folic acid-cysteamine modified gold nanoparticle as a nanoprobe for targeted computed tomography imaging of cancer cells. Mater. Sci. Eng. C 89, 182–193.
Lee, N., Choi, S.H., Hyeon, T., 2013. Nano-sized CT contrast agents. Adv. Mater. 25, 2641–2660.
Liu, H., Xu, Y., Wen, S., Chen, Q., Zheng, L., Shen, M., et al., 2013. Targeted tumor computed tomography imaging using low-generation dendrimer-stabilized gold nanoparticles. Chem. Eur. J. 19, 6409–6416.
Long, Z., Liu, M., Wang, K., Deng, F., Xu, D., Liu, L., et al., 2016. Facile synthesis of AIE-

active amphiphilic polymers: self-assembly and biological imaging applications. Mater. Sci. Eng. C 66, 215–220.
Lu, X., Lin, J., Qin, J., Peng, C., 2016. Folic acid-modified diatrizoic acid-linked dendrimer-entrapped gold nanoparticles as nanoprobes for targeted CT imaging of human cervical cancer. Nanomed. J. 3.
Mankoff, D.A., 2007. A definition of molecular imaging. J. Nucl. Med. 48, 18N–21N.
Mao, L., Liu, Y., Yang, S., Li, Y., Zhang, X., Wei, Y., 2018. Recent advances and progress of fluorescent bio-/chemosensors based on aggregation-induced emission molecules. Dye. Pigment. 162, 611–623.
Missbach-Guentner, J., Hunia, J., Alves, F., 2011. Tumor blood vessel visualization. Int. J. Dev. Biol. 55 (4–5), 535–546.
Mohandes, F., Salavati-Niasari, M., 2014a. Freeze-drying synthesis, characterization and in vitro bioactivity of chitosan/graphene oxide/hydroxyapatite nanocomposite. RSC Adv. 4, 25993–26001.
Mohandes, F., Salavati-Niasari, M., 2014b. In vitro comparative study of pure hydroxyapatite nanorods and novel polyethylene glycol/graphene oxide/hydroxyapatite nanocomposite. J. Nanoparticle Res. 16, 2604.
Peng, C., Qin, J., Zhou, B., Chen, Q., Shen, M., Zhu, M., et al., 2013. Targeted tumor CT imaging using folic acid-modified PEGylated dendrimer-entrapped gold nanoparticles. Polym. Chem. 4, 4412–4424.
Samadian, H., Hosseini-Nami, S., Kamrava, S.K., Ghaznavi, H., Shakeri-Zadeh, A., 2016. Folate-conjugated gold nanoparticle as a new nanoplatform for targeted cancer therapy. J. Cancer Res. Clin. Oncol. 142, 2217–2229.
Thakur, M.L., Lentle, B.C., 2005. Joint SNM/RSNA molecular imaging summit statement. J. Nucl. Med. 46, 11N–13N.
Wang, H., Zheng, L., Peng, C., Shen, M., Shi, X., Zhang, G., 2013. Folic acid-modified dendrimer-entrapped gold nanoparticles as nanoprobes for targeted CT imaging of human lung adencarcinoma. Biomaterials 34, 470–480.
Xu, C., Wang, Y., Zhang, C., Jia, Y., Luo, Y., Gao, X., 2017. AuGd integrated nanoprobes for optical/MRI/CT triple-modal in vivo tumor imaging. Nanoscale 9, 4620–4628.
Zhang, X., Wang, K., Liu, M., Zhang, X., Tao, L., Chen, Y., Wei, Y., 2015. Polymeric AIE-based nanoprobes for biomedical applications: recent advances and perspectives. Nanoscale 7, 11486–11508.
Zhou, B., Yang, J., Peng, C., Zhu, J., Tang, Y., Zhu, X., et al., 2016. PEGylated polyethylenimine-entrapped gold nanoparticles modified with folic acid for targeted tumor CT imaging. Colloids Surf. B Biointerfaces 140, 489–496.